IOP Publishing Quantum Sci. Technol. 8 (2023) 045006 https://doi.org/10.1088/2058-9565/ace54b

Quantum Science and Technology

OPEN ACCESS

RECEIVED
23 December 2022

REVISED
25 April 2023

ACCEPTED FOR PUBLICATION
7 July 2023

PUBLISHED
20 July 2023

PAPER

High-efficiency photon-number-resolving detector for improving heralded single-photon sources

Lorenzo Stasi[1,2,3,*], **Patrik Caspar**[1,3], **Tiff Brydges**[1], **Hugo Zbinden**[1], **Félix Bussières**[2] and **Rob Thew**[1]

[1] Department of Applied Physics, University of Geneva, CH-1211 Geneva, Switzerland
[2] ID Quantique SA, CH-1227 Geneva, Switzerland
[3] L S and P C contributed equally to this work.
[*] Author to whom any correspondence should be addressed.

E-mail: lorenzo.stasi@idquantique.com

Keywords: SNSPD, photon number resolution, heralded single-photon sources

Abstract

Heralded single-photon sources (HSPS) intrinsically suffer from multiphoton emission, leading to a trade-off between the source's single-photon quality and the heralding rate. A solution to this problem is to use photon-number-resolving (PNR) detectors to filter out the heralding events where more than one photon pair is created. Here, we demonstrate an improvement of a HSPS by heralding photons using a high-efficiency parallel superconducting nanowire single-photon detector (P-SNSPD) with PNR power. Specifically, we show a reduction in the $g^{(2)}(0)$ of the heralded single photon by $(26.9 \pm 0.1)\%$ for a fixed pump power, or alternatively, an increase in the heralding rate by a factor of 1.368 ± 0.002 for a fixed $g^{(2)}(0)$. We also demonstrate that such a PNR device can reveal thermal photon-number statistics of unheralded photons, which is enabled by our ability to construct its full input–output response function. These results are possible thanks to our P-SNSPD architecture that ensures non-latching operation with no electrical crosstalk, which are essential conditions necessary to obtain the correct photon-number statistics and also faster recovery times, therefore enabling fast heralding rates. These results show that our efficient PNR P-SNSPD architecture can significantly improve the performance of HSPSs and can precisely characterize them, making these detectors a useful tool for a wide range of optical quantum information protocols.

1. Introduction

Over the past decades, there have been remarkable developments in the field of quantum technologies. In particular, photonic systems employing single photons have been used in a variety of applications, ranging from quantum communication and repeater protocols [1, 2] to linear optical quantum computing [3–5] and Gaussian boson sampling [6–8]. A convenient and versatile tool to generate single photons are heralded single-photon sources (HSPS) [9, 10]. They have the advantage of operating at room temperature, are wavelength and bandwidth tunable, and can produce indistinguishable and pure photons [11–13].

The photon generation mechanism in HSPSs is, however, probabilistic and multi-photon events can also occur. Such events are undesired, leading to a decrease in the single-photon fidelity [14]. Therefore, to minimize their impact, HSPSs are often used in the low-squeezing regime ($\mu \ll 1$, where μ is the mean photon-pair number per pump pulse). However, in such a regime the probability of emitting vacuum states increases, reducing the generation rate of single photons.

A possible solution to this problem is to use a photon-number resolving (PNR) detector as the heralding detector. In this way, it is possible to filter out events when more than one photon is detected, therefore lowering the multi-photon contribution in the heralded state. In principle, such a scheme would allow one to work with a higher μ, making it possible to increase the heralding rate towards the theoretical limit of 25% of the pump rate [15].

Transition-edge sensors (TES) have shown to be able to distinguish high numbers of photons with high probability [16, 17]. However, the long recovery time of several microseconds precludes their application in high rate experiments, limiting their operation to the hundreds of kHz regime. In addition, TESs need ultra-low temperatures ($<$100 mK) which requires a complex cryogenic system.

Recently, superconducting nanowire single-photon detectors (SNSPD) have demonstrated few-photon PNR capability based on the signal's slew rate [18] or on the amplitude of the voltage pulse when used in combination with an impedance-matching taper [19]. Both methods have been employed in recent experiments to improve the heralded $g^{(2)}(0)$ measurement of HSPSs [20, 21]. In the first approach, one can either fit the waveform's rising edge or use a differentiating circuit to retrieve the photon-number event, which requires detectors with very low timing jitter. In the second scenario, the impedance-matching taper acts as a kinetic inductive element, which increases the recovery time of the overall detector, potentially limiting its usage at high repetition rates. Additionally, to be able to resolve photon-number states, photons need to arrive with minimum delay between each other, limiting light pulses to tens of ps [19].

A promising alternative technology is based on SNSPDs in a parallel configuration (P-SNSPD) [22–24]. This consists of an array of several pixels (the single SNSPD element) which are electrically connected in parallel. With respect to an array of independent pixels, which would require one coaxial cable per pixel for the read-out, a P-SNSPD requires only one, which is a practical advantage. In fact, information on the number of pixels that clicked can be extracted directly from the signal amplitude's only, so a full digitalization and analysis of the trace or fast and precise electronics are not necessary, which can ease the photon-number discrimination process. Hence, a P-SNSPD can be used with any discriminator-based time-tagging device. In addition, the active detection area covered by the P-SNSPD is the same as a single-meander SNSPD, resulting in pixels of shorter length that can recover faster thanks to the lower kinetic inductance.

However, ensuring that a P-SNSPD operates correctly is not a trivial task. In fact, many effects can occur which would alter the experimental results: thermal crosstalk, electrical crosstalk and latching. The common solution is to operate the detector at a lower bias current to mitigate the thermal crosstalk and the current redistribution effect that causes the electrical crosstalk (and possibly latching). However, such a solution is not effective at high count rates and, more importantly, it lowers the system detection efficiency of the device, which is clearly non-ideal for optimal operation of a HSPS. In order to solve these problems altogether, we developed a novel P-SNSPD design that can reach high detection efficiency and high detection rate in a latch-free regime, while operating the detector at the optimal bias current value. Detailed information of this architecture can be found in [23]. We also investigated the PNR performance of our novel P-SNSPD design in [24], where the full input–output response function of the detector is obtained thanks to the development of a new analytical model that describes the multi-photon detection probabilities. Therefore, thanks to such developments, our P-SNSPD can be used to measure photon-number statistics in high repetition rate regimes.

Another important aspect regarding single-photon sources is the characterization of their emission statistics. More generally speaking, it is paramount to understand if a particular quantum system may suffer from multi-photon emission (as a thermal source does) and to quantify it [25–27]. To this end, one needs a PNR detector with a fully mapped input–output response function that displays a clear distinction between the different generated signals in order to correctly assign each one of them to the corresponding photon-count event (as a P-SNSPD does). In fact, it is only in this way that it is possible to correctly reconstruct the emitting light statistics of a source.

This paper reports on the improvements to a HSPS that can be achieved through the use of a high ($>$80%) single-photon-efficiency P-SNSPD, when used to distinguish multi-photon detection events. We first introduce the theoretical tools that we use to describe the employed source and the detectors. Then we conduct two experiments, first we show the improvement from using the P-SNSPD as a heralding detector as part of a HSPS with regard to improving the $g^{(2)}(0)$ of the heralded single-photon state. Second, we show that a P-SNSPD can be used to correctly measure and reconstruct the thermal statistics of the HSPS. We benchmark our result by retrieving the unconditional $g^{(2)}(0)$ on a single spatial mode. This result demonstrates that our P-SNSPD can be used as a quantum metrology tool for source characterization [25–27].

2. Theory

The ideal state generated by a spontaneous parametric down-conversion (SPDC) source is a two-mode squeezed vacuum (TMSV) state described by [28]

$$|\Psi\rangle_{\mathrm{si}} = \sqrt{1-\lambda^2}\sum_{n=0}^{\infty}\lambda^n|nn\rangle_{\mathrm{si}} = \sum_{n=0}^{\infty}\sqrt{\frac{\mu^n}{(\mu+1)^{n+1}}}|nn\rangle_{\mathrm{si}}, \tag{1}$$

where $\lambda = \tanh(r)$ with the squeezing parameter r and the mean photon number $\mu = \sinh^2(r) = \lambda^2/(1-\lambda^2)$. Note that the marginal states of the signal (s) and idler (i) modes are thermal states with photon-number probability distribution

$$p_n = \frac{\mu^n}{(\mu+1)^{n+1}}. \tag{2}$$

A standard measurement to probe a SPDC source is represented by the second-order autocorrelation function [28]

$$g^{(2)}(0) = \frac{\langle\hat{n}(\hat{n}-1)\rangle}{\langle\hat{n}\rangle^2} = \frac{\sum_n n(n-1)p_n}{\left(\sum_n np_n\right)^2}, \tag{3}$$

where $\hat{n}$ is the photon-number operator and p_n the photon-number probability distribution of the state. To this end, two different measurements can be performed on a SPDC source, unconditional and heralded $g^{(2)}(0)$. The former is measured on one mode of the state and gives information on the statistical nature of a source and on the spectral purity of the generated photons. The latter instead is measured on one mode given a heralding detection on the other mode of the state and quantifies the amount of multi-photon pairs that are generated from the SPDC source.

First, we consider the scenario shown in figure 1(a), in which the signal photon is sent to a P-SNSPD acting as a heralding detector, $\mathrm{D_h}$, and the idler photon is sent to a 50/50 beam splitter followed by two threshold SNSPDs, $\mathrm{D_a}$ and $\mathrm{D_b}$, which are only able to distinguish between 0 or at least one photon. In order to obtain analytical equations describing the single and coincidence detection probabilities per pump pulse, we use the approach of [29]. In this formalism, the TMSV state $\rho = |\Psi\rangle\langle\Psi|_{\mathrm{si}}$ can be expressed as 4×4 covariance matrix with μ as a single free parameter. Furthermore, the action of beam splitters can be modeled by Gaussian unitary operations. The formalism additionally allows modes to be traced out, and so we are able to model transmission loss on a given mode by introducing an auxiliary mode, applying a beam splitter operation between the two modes, and finally tracing out the auxiliary mode. Moreover, the formalism also allows for calculation of the expectation value of a given Gaussian state after projection onto vacuum. Therefore, we can model threshold detectors described by positive-operator-valued measure (POVM) elements $E_0 = |0\rangle\langle0|$ corresponding to a no-click outcome and $E_{\mathrm{c}} = \mathbb{1} - |0\rangle\langle0|$ to a click outcome. To obtain a model for the P-SNSPD, we note that each of the N pixels of the detector is a threshold detector. Therefore, a physically intuitive model for the P-SNSPD consists of a sequence of beam splitters, with splitting ratios corresponding to the characterized pixel efficiencies, and N threshold detectors (see appendix A for further details).

To additionally take account of the non-unit spectral purity of our source, we assume a multimode state $\rho = \varrho_1 \otimes \cdots \otimes \varrho_M$. Here $\varrho_k = |\Psi\rangle\langle\Psi|_k$, as defined in equation (1), describes a single Schmidt mode with mean photon number $\lambda_k\mu$, where the Schmidt coefficients are normalized such that $\sum_k \lambda_k = 1$. In the case of a SPDC source, the Schmidt coefficients can be estimated by a measurement of the joint spectral intensity [30]. In this way, we obtain a model to accurately describe the expected single and coincidence detection probabilities per pump pulse and the heralded $g^{(2)}(0)$

$$g_{\mathrm{h}}^{(2)}(0) \approx \frac{p_{\mathrm{h}}p_{\mathrm{hab}}}{p_{\mathrm{ha}}p_{\mathrm{hb}}}, \tag{4}$$

where p_{h} is the probability of a heralding detection, $p_{\mathrm{ha(b)}}$ the probability of a coincidence detection between detectors $\mathrm{D_h}$ and $\mathrm{D_a}$ ($\mathrm{D_b}$), and p_{hab} the triple-coincidence probability between $\mathrm{D_h}$, $\mathrm{D_a}$, and $\mathrm{D_b}$. For details on the derivation and the explicit formulas for the probabilities, see appendix A.

Similarly, the unconditional $g^{(2)}(0)$ on one spatial mode of the TMSV state can be evaluated as

$$g_{\mathrm{unc.}}^{(2)}(0) \approx \frac{p_{\mathrm{ab}}}{p_{\mathrm{a}}p_{\mathrm{b}}}, \tag{5}$$

where $p_{\mathrm{a(b)}}$ is the probability of a detection on $\mathrm{D_a}$ ($\mathrm{D_b}$) and p_{ab} the probability of a coincidence detection between $\mathrm{D_a}$ and $\mathrm{D_b}$. We note that in the case where we have direct access to the photon-number probability distribution p_n of the state, e.g. by measuring it with a PNR detector, one can also use equation (3) to obtain $g_{\mathrm{unc.}}^{(2)}(0)$.

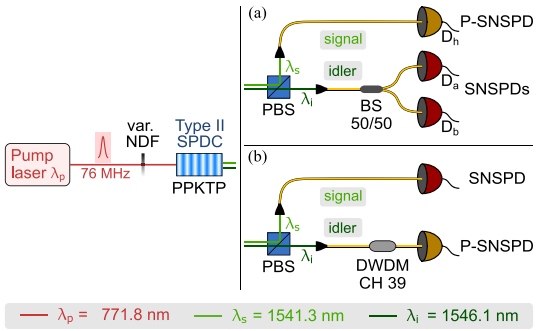

Figure 1. Experimental setups used for the two different measurements of (a) heralded $g^{(2)}(0)$ and (b) unconditional $g^{(2)}(0)$. A Ti:sapphire laser in the picosecond pulsed regime at $\lambda_p = 771.8$ nm with a repetition rate of 76 MHz is used to pump a 30 mm long periodically poled potassium titanyl phosphate (PPKTP) bulk nonlinear crystal with poling period $\Lambda = 46.2\,\mu$m. In this way, non-degenerate signal ($\lambda_s = 1541.3$ nm) and idler ($\lambda_i = 1546.1$ nm) photon pairs are generated via type-II SPDC, where the pump power can be varied with a reflective variable neutral density filter (NDF). Signal and idler photons are separated by a polarizing beam splitter (PBS) and coupled into single-mode optical fibers. (a) The heralding signal photons are detected by the P-SNSPD while the idler photons are sent to a 50/50 beam splitter (BS) and detected by threshold SNSPDs. (b) The idler photons are spectrally filtered by a dense wavelength division multiplexer (DWDM) channel 39 and detected by the P-SNSPD for the reconstruction of the thermal photon number statistics.

3. Experiment

In a first experiment, as illustrated in figure 1(a), we employ a P-SNSPD as the heralding detector in a HSPS and assess its performance by measuring $g_{\mathrm{h}}^{(2)}(0)$ for different pump power settings. We use the P-SNSPD in two different configurations: as a threshold detector, where all the $(n \geqslant 1)$-click events are considered as a (single) detection, and as a PNR detector, where only $(n = 1)$-click events are considered.

In a second experiment, shown in figure 1(b), we replace the 50/50 beam splitter and the two standard SNSPDs by a single P-SNSPD to reconstruct the photon-number probability distribution. Using equation (3) we calculate $g_{\mathrm{unc.}}^{(2)}(0)$ and compare it to the values obtained when using the more standard method, where a 50/50 beam splitter and two threshold detectors are used, via equation (5). Here, we additionally filter the idler mode with a dense wavelength division multiplexer in order to obtain spectrally pure photons and suppress leaking signal photons due to the finite extinction ratio of the polarizing beam splitter which separates the signal and idler photons.

The spectral purity of the heralded single photons is characterized by a joint spectral intensity measurement [30, 31] and was found to be ∼84%. For increasing pump power, we observe a decrease in purity due to spectral broadening of the pump light caused by the non-linearity of the spatial mode cleaning fiber (Coherent 780 HP, 9 cm long) before the PPKTP crystal. We take this into account for our theory model by fitting equation (5) to the experimental data with the purity P as a fit parameter, see appendix A.

The total efficiencies (including transmission, coupling and detection efficiencies) are measured in the setup shown in figure 1(a) at low pump power ($\mu \approx 5 \times 10^{-4}$) using the method described in [32]. We obtain the values $\eta_{\mathrm{h}} = (C_{\mathrm{ha}} + C_{\mathrm{hb}})/(C_{\mathrm{a}} + C_{\mathrm{b}}) = 0.6348(5)$, $\eta_{\mathrm{a}} = 2C_{\mathrm{ha}}/C_{\mathrm{h}} = 0.6293(6)$ and $\eta_{\mathrm{b}} = 2C_{\mathrm{hb}}/C_{\mathrm{h}} = 0.5809(6)$, where C denotes the (coincidence) counts (conditioned on the pump pulse in 1 ns window) on the corresponding detectors within 3 min of integration time. Note that the efficiencies η_{a} and η_{b} do not include the 50/50 beam splitter. Dark counts are negligible (<100 counts per second for all detectors) and do not affect the measurements.

The two standard threshold detectors are in-house developed single-pixel SNSPDs made from molybdenum silicide (MoSi) and have system detection efficiencies of about 85% and 83%, respectively. The P-SNSPD consists of four adjacent MoSi pixels, where the amplitude of the electrical readout signal is dependent on the number of pixels that click in the detection process. To avoid electrical and thermal crosstalk between the pixels, we employed the architecture developed in [23]. In order to characterize the full input–output response function of the P-SNSPD, light with known statistics (Poissonian with $\mu = 1$, in our case) is sent onto the detector. The photon-counting statistics are collected and, by employing the analytical model described in [24], one can obtain the conditional probability matrix $\mathbf{P}$. Its elements P_{nm} denote the probabilities of registering an n-click event when m photons are incident on the detector. Therefore, an initial photon-number probability distribution p_m leads to an n-click probability recorded by the P-SNSPD of $q_n = \sum_{m=0}^{\infty} P_{nm} p_m$. Even though m can go to infinity, practically it is stopped at a finite value M. Therefore, $\mathbf{P}$ has dimension $(N+1) \times (M+1)$, where N is the number of pixels of the P-SNSPD. By inverting $\mathbf{P}$, the incident photon-number probability distribution p_m can be reconstructed from the detected click probability

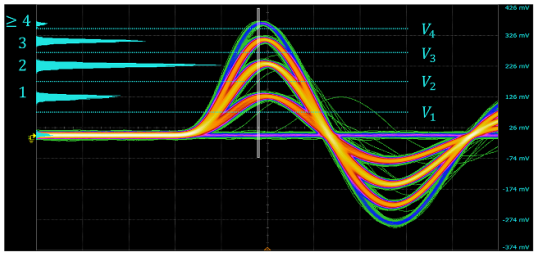

Figure 2. Oscilloscope persistence traces of the electrical signals generated by the P-SNSPD (500 ps div^{-1} and 100 mV div^{-1}). On the left, are reported the waveforms histograms corresponding to each n-click event, taken from the vertical white slice. The n-click events are discriminated by setting different voltage thresholds on the time tagger.

distribution q_n. In our case for $N = 4$ and $M = 9$, we measured $P_{11} = 84\%$, $P_{12} = 55\%$, $P_{22} = 42\%$, $P_{13} = 31\%$ and $P_{14} = 17\%$ (the full **P** matrix can be found in appendix B). The time taken for a full recovery of the efficiency after a detection is <40 ns and is obtained by measuring the probability distribution of the time between two consecutive detections [24].

For the photon-number discrimination, the electrical readout signal of the P-SNSPD is separated in two by a coaxial power splitter and discriminated by a time controller (ID Quantique, ID900) at two different voltage thresholds, corresponding to a detection of $n \geqslant 1$ photons and $n \geqslant 2$ photons (see figure 2). In the second experiment, where the photon-number probability distribution is reconstructed, we also use a third discrimination level corresponding to a detection of $n \geqslant 3$ photons. The time controller additionally takes the electrical pickup signal from the pump laser and the readout signals from the threshold SNSPDs. All detection events are taken within a 1 ns time window with respect to the pump pulses to reduce dark count contributions, and their timestamps are saved for the data analysis.

4. Results

The results of the first experiment (see figure 1(a)), where we use the P-SNSPD as the heralding detector for the HSPS, are shown in figure 3. We calculate the mean photon number μ from the measured probability of detecting a heralding photon, p_{h}, in the threshold configuration together with the characterized total efficiency of the heralding photons η_{h} and the Schmidt coefficients λ_k obtained from a fit of equation (5) to the corresponding measured data (see equation (A1) in appendix A). The values for $g_{\mathrm{h}}^{(2)}(0)$ are calculated according to equation (4), where the blue points correspond to the threshold configuration of the P-SNSPD and the red points to the PNR configuration. The solid lines are obtained from the theoretical model described in section 2 with the characterized total efficiencies η_{h}, η_{a}, η_{b} and λ_k as defined in section 3. The shaded areas around the solid lines mark the regions with a difference in spectral purity of $\pm 4\%$ and the dashed lines show the theory calculation for a spectrally pure source.

The ratio between the blue and the red data is $g_{\mathrm{h,thr}}^{(2)}(0)/g_{\mathrm{h,PNR}}^{(2)}(0)$ which is the factor by which the heralding rate can be increased when switching from threshold to PNR heralding mode while keeping a fixed $g_{\mathrm{h}}^{(2)}(0) \ll 1$. In our experiment, we obtain 1.368 ± 0.002, averaged across all μ values, which inversely corresponds to a reduction in $g_{\mathrm{h}}^{(2)}(0)$ of 26.9(1)%. It should be noted that, in this demonstration, no spectral filtering of the heralding photons has been performed, in order to show the maximum achievable improvement in $g_{\mathrm{h}}^{(2)}(0)$ with our PNR detector.

As described in section 3, in the second experiment (see figure 1(b)) we reconstruct the photon-number probability distribution of one mode of the TMSV state by measuring the click probability distribution with the P-SNSPD. We then calculate $g_{\mathrm{unc.}}^{(2)}(0)$ using equation (3) and compare it to the value obtained by the standard method using equation (5). The results for different mean photon numbers are shown in figure 4 and display $g_{\mathrm{unc.}}^{(2)}(0) \approx 2$ which confirms the thermal nature of our source.

The error bars for the P-SNSPD are calculated through a Monte Carlo method with 10^3 iterations. In each iteration, to characterize **P**, the Poissonian input state used for the detector characterization is randomly picked from a Gaussian distribution centered at $\mu = 1$ (the experimental value) with a standard deviation of $\sigma = 0.05$. In this way, we take into account the uncertainties of our characterization setup (see [24] for more details). The obtained matrix **P** is then used to reconstruct the light input statistics p_m of the SPDC source from the experimental photon-counting distribution of the P-SNSPD. As a last step in each iteration, the value $g_{\mathrm{unc.}}^{(2)}(0)$ is computed from the reconstructed statistics using equation (3).

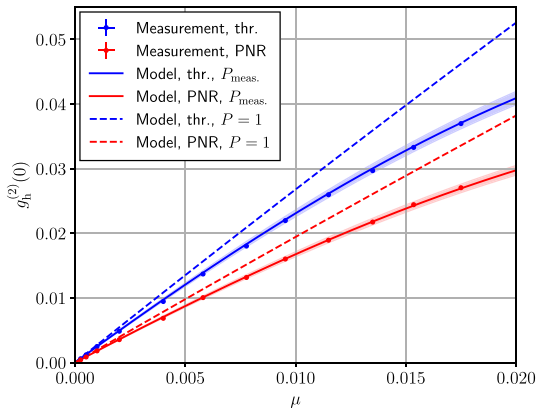

Figure 3. Heralded second-order autocorrelation function as a function of the mean photon number μ. The blue points correspond to the case where the P-SNSPD operates in threshold configuration (thr.), whereas the red points show the measurements for PNR configuration. The solid lines are obtained from the theoretical model with the same purity as in the experiment, where the shaded areas mark the spectral purity interval of ±4%. The dashed lines show the behavior for a source with purity $P = 1$.

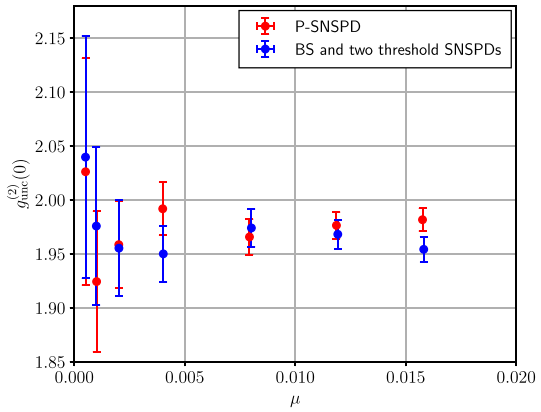

Figure 4. Unconditional second-order autocorrelation measurement on the spectrally filtered idler mode of the SPDC source. The red data correspond to the measurement with the P-SNSPD, whereas the blue data are obtained with the standard method using a beam splitter and two threshold detectors.

5. Discussion

In order to improve the HSPS, the most important parameters to optimize are the PNR capability of the detector and the total efficiency of the heralding photons η_{h}, i.e. transmission through optical elements, coupling and detection efficiency [20]. As shown in figure 5, for a pure SPDC source combined with an ideal PNR heralding detector ($\mathbf{P} = \mathbb{1}$), the reduction in $g_{\text{h}}^{(2)}(0)$, that is $1 - g_{\text{h,PNR}}^{(2)}(0)/g_{\text{h,thr}}^{(2)}(0)$, reaches 100% for $\eta_{\text{h}} = 1$. It achieves a value of 50% for $\eta_{\text{h}} = 0.67$ and surpasses 90% for $\eta_{\text{h}} = 0.95$. For $\eta_{\text{h}} = 0.635$, as measured in our experiment, a perfect PNR detector would achieve a reduction of 46.5%, however, our reported value of 26.9(1)% lies significantly lower. This is due to the fact that the PNR capability of the detector to correctly detect an incoming higher-photon-number state is still limited by the non-resolvability of two photons hitting the same pixel. Another possible cause is the non-unit efficiency of the detector: it is possible that if two photons arrive on two different pixels, only one is detected. In order to increase the PNR capability of our P-SNSPD, the number of pixels needs to be increased while still maintaining good amplitude discrimination of the electrical readout signal between different photon-number detection events. In addition, a uniform light distribution over the pixels can be obtained by exploiting an interleaved design, which reduces the probability of having more photons arriving at the same pixel [33] (e.g. for the same single-photon-detection-efficiency, the P_{22} would become 53%). To give more context, by exchanging our P-SNSPD with the recently reported multi-pixel detector [34] composed of 14 interleaved pixels, the achievable $g_{\text{h}}^{(2)}(0)$ reduction would be 47%.

Lastly, we show that P-SNSPDs can correctly reconstruct the thermal statistics of an SPDC source thanks to our access to the full $\mathbf{P}$ matrix and the clear distinction between each photon-count signal. To validate our

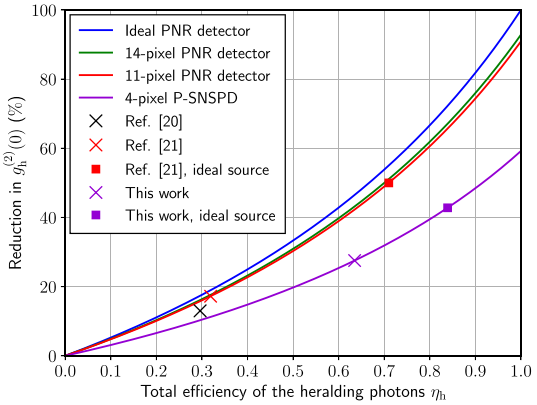

Figure 5. Reduction in $g_h^{(2)}(0)$ as a function of the total efficiency of the heralding photons η_h. The solid lines are obtained from the theoretical model for a spectrally pure source with fixed $\mu = 10^{-3}$. For the 14- and 11- pixel PNR detectors, we assume uniform light distribution across the pixels. The crosses are calculated from the measured values and the squares are obtained by assuming unit efficiency on the source side, i.e. $\eta_h = P_{11}$.

Table 1. Comparison of different parameters between PNR SNSPDs used to improve a HSPS. The heralded single-photon rates R_{hsp} are calculated from a fit to the measured data at $\mu = 0.005$ and have been estimated for the other references. For [20], we assume η_a and η_b equal to η_h, since their values were not reported.

References	PNR method	P_{11}	P_{12}	P_{22}	Full recovery time	η_h	$g_h^{(2)}(0)$ reduction	R_{hsp}(kcps)	Pump rate (MHz)
[20]	Slew rate	80%–86%	—	—	<100 ns	29.6%	13%	4.4	10
[21]	Slew rate	71%	45.8%	45.8%	100 ns	31.9%	20%	0.64	1
This work	Signal's amplitude	84%	55%	42%	<40 ns	63.5%	26%	146	76

results, we retrieve the unconditional $g^{(2)}(0)$ values via equation (3). As it can be seen from the results, the $g_{unc.}^{(2)}(0)$ obtained with the two different techniques match very well, both in the absolute value and in the amplitude of the error bars. This result demonstrates that P-SNSPDs can effectively replace a 50/50 beam splitter and two detectors used in the standard method, simplifying the overall experimental apparatus. Hence, they can for example be applied in protocols which require upper bounds on the probability of having more than one photons in each spatial mode [2, 35]. It is important to note that the approach does not rely on an accurate absolute characterization of the P-SNSPD efficiency, keeping the $g_{unc.}^{(2)}(0)$ measurement efficiency-independent as in the case of the more common-place method which uses two detectors. However, this is not the case for the reconstructed photon-number distribution, p_n.

In table 1, and additionally in figure 5, we compare the main results of this work with [20, 21], which also employ a PNR SNSPD to improve a HSPS. We report a significant $g_h^{(2)}(0)$ reduction thanks to the high value of η_h in our experiment and the good P_{22} value of the P-SNSPD. Furthermore, our heralded single-photon rate (R_{hsp}) for a value of $\mu = 0.005$ is over 30 times higher than the rates reported in the previous works. This result is mainly due to the high pump repetition rate assisted by the fast detector recovery time that the P-SNSPD can sustain in the operationally relevant low squeezing regime. Increasing the number of pixels could further improve the results we obtain, both in terms of P_{22} and recovery time, which would reflect in a better $g_h^{(2)}(0)$ reduction and higher heralded single-photon rate.

6. Conclusion

We have shown the benefit for a HSPS that a PNR detector, such as a P-SNSPD, can bring when combined with a SPDC source. Even though P-SNSPDs do not possess perfect PNR capability, we already demonstrate a significant reduction in the heralded $g^{(2)}(0)$ of 26.9(1)%, compared to the threshold configuration. In addition, the PNR capability of the P-SNSPD is not limited by the timing jitter as in the case of a slew rate discrimination, or by super-short light pulses (tens of ps) as in the impedance-matching taper approach. Lastly, to improve our results further, the number of pixels of the P-SNSPD need to be increased. In that case, not only a better photon-number discrimination can be achieved, but also an overall faster recovery time, thanks to the shorter meanders of the P-SNSPD structure. This result marks a first step towards high-rate generation of single photons which could be of use in repeater protocols [36]. We further show the usefulness

of our P-SNSPD for the task of reconstructing the photon-number probability distribution of pulsed light by measuring a thermal state. We demonstrated that we can estimate $g^{(2)}(0)$ with a single detector, which replaces a beam splitter and two threshold detectors used in more common methods. Therefore, such a PNR detector can be of great help in quantum protocols, metrology applications, and source characterization.

Data availability statement

All data that support the findings of this study are included within the article (and any supplementary files).

Acknowledgments

We thank Giovanni V Resta and Gaëtan Gras for useful discussions. This work was supported by the Swiss National Science Foundation SNSF (Grant No. 200020_182664) and by NRC CSTIP Grant QSP043. L S is part of the AppQInfo MSCA ITN which received funding from the EU Horizon 2020 research and innovation program under the Marie Sklodowska-Curie Grant Agreement No. 956071.

Appendix A. Theoretical model

We use a characteristic function based approach to model our SPDC source and to derive the single and coincidence detection probabilities [29]. We start with the covariance matrix of a TMSV state and apply Gaussian unitary operations corresponding to the action of the beam splitters in our model as shown in figure 6. On each mode, we apply a loss channel with the corresponding transmittance η_a, η_b and η_h. Each detector is described by a POVM with element $E_0 = |0\rangle\langle 0|^{\otimes M}$ corresponding to a no-click outcome and $E_c = \mathbb{1} - |0\rangle\langle 0|^{\otimes M}$ corresponding to a click outcome over all the spectral modes M. This leads to the following detection probability of a detecting a heralding photon per pump pulse

$$p_h = \sum_{k=1}^{N} \mathrm{tr}\rho\left(\mathbb{1}_a \otimes \mathbb{1}_b \otimes E_{c,h_k} \otimes E_{0,h_{\neg k}}^{\otimes(N-1)}\right) = \sum_{k=1}^{N}\left(\prod_m \frac{1}{1+(1-T_k)\eta_h\lambda_m\mu}\right) - N\prod_m \frac{1}{1+\eta_h\lambda_m\mu}, \tag{A1}$$

where $\{\lambda_m\}_{m=1}^{M}$ denote the Schmidt coefficients (with $\sum_m \lambda_m = 1$) and T_k is the fraction of the light that reaches pixel k of the heralding detector with $\sum_k T_k = 1$. Note that here and in the following, taking $\{T_k\}_{k=1}^{N}$ models a single-photon detection event on the P-SNSPD, but by setting $N = 1$ and $T_1 = 1$ one obtains the behavior for the detector in threshold configuration, i.e. detecting one or more photons.

Similarly to p_h, we obtain the probability of a coincidence detection between the heralding detector D_h and detector D_a after the 50/50 beam splitter on the heralded mode

$$\begin{aligned} p_{ha} &= \sum_{k=1}^{N} \mathrm{tr}\rho\left(E_{c,a} \otimes \mathbb{1}_b \otimes E_{c,h_k} \otimes E_{0,h_{\neg k}}^{\otimes(N-1)}\right) \\ &= p_h - \sum_{k=1}^{N}\left(\prod_m \frac{2}{2+[(1-T_k)(2-\eta_a)\eta_h+\eta_a]\lambda_m\mu}\right) + N\prod_m \frac{2}{2+[(2-\eta_a)\eta_h+\eta_a]\lambda_m\mu} \end{aligned} \tag{A2}$$

and the three-fold coincidence probability

$$\begin{aligned} p_{hab} &= \sum_{k=1}^{N} \mathrm{tr}\rho\left(E_{c,a} \otimes E_{c,b} \otimes E_{c,h_k} \otimes E_{0,h_{\neg k}}^{\otimes(N-1)}\right) \\ &= p_{ha} + p_{hb} - p_h + \sum_{k=1}^{N}\left(\prod_m \frac{2}{2+[(1-T_k)(2-\eta_a-\eta_b)\eta_h+\eta_a+\eta_b]\lambda_m\mu}\right) \\ &\quad - N\prod_m \frac{2}{2+[(2-\eta_a-\eta_b)\eta_h+\eta_a+\eta_b]\lambda_m\mu}. \end{aligned} \tag{A3}$$

The detection probability of detector D_a (and similarly for detector D_b) is given by

$$p_a = \sum_{k=1}^{N} \mathrm{tr}\rho\left(E_{c,a} \otimes \mathbb{1}_b \otimes \mathbb{1}_h^{\otimes N}\right) = 1 - \prod_m \frac{1}{1+\eta_a\lambda_m\mu} \tag{A4}$$

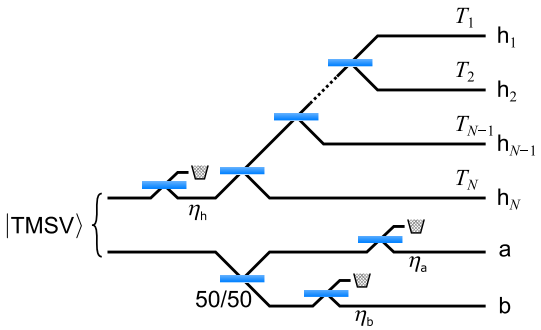

Figure 6. Schematic representation of the theory model to calculate the single and coincidence detection probabilities. The heralding mode of the two-mode squeezed vacuum (TMSV) state is subject to loss (η_h) and is then split into N modes before being detected by threshold detectors (h_1 to h_N) on each mode. The other mode of the TMSV state is sent to a 50/50 beam splitter and further undergoes loss channels (η_a and η_b) before reaching the threshold detectors D_a and D_b.

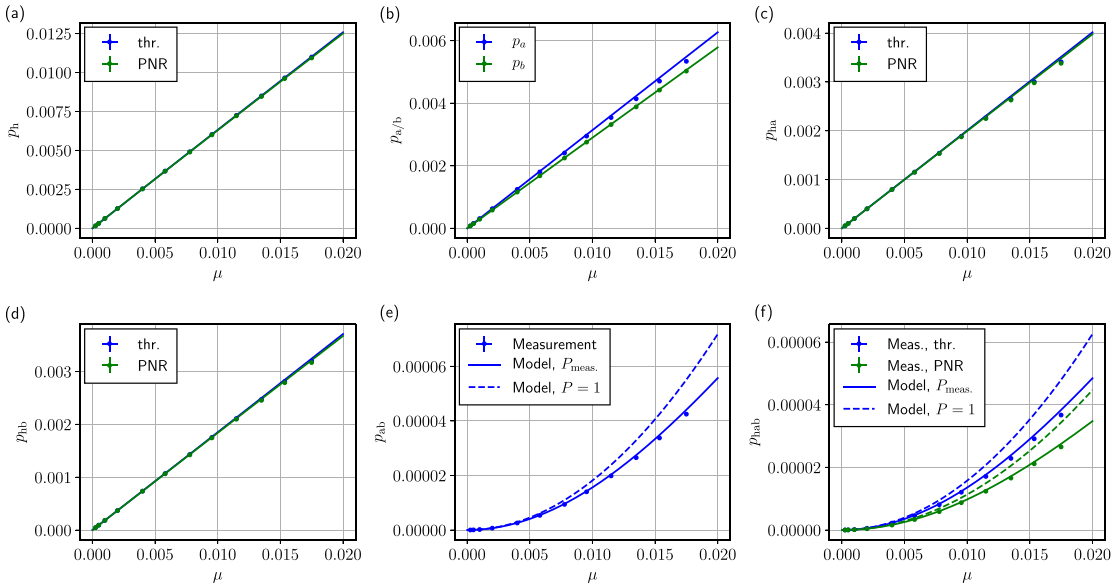

Figure 7. Measurement and theory model for the single and coincidence detection probabilities. The solid lines are obtained from the theory model including the non-unit purity of our SPDC source whereas the dashed lines describe the behavior for a pure source. (a) Probability of a heralding detection per pump pulse for the threshold and PNR configurations. (b) Detection probabilities for detectors D_a and D_b. (c) Coincidence probability between detectors D_h and D_a. (d) Coincidence probability between detectors D_h and D_b. (e) Coincidence probability for detections on D_a and D_b. (f) Triple-coincidence probability between detectors D_h, D_a and D_b.

and the coincidence probability between detector D_a and D_b by

$$p_{ab} = \sum_{k=1}^{N} \mathrm{tr}\rho\left(E_{c,a} \otimes E_{c,b} \otimes \mathbb{1}_h^{\otimes N}\right) = 1 - \prod_m \frac{2}{2+\eta_a\lambda_m\mu} - \prod_m \frac{2}{2+\eta_b\lambda_m\mu} + \prod_m \frac{2}{2+(\eta_a+\eta_b)\lambda_m\mu}. \quad \text{(A5)}$$

Those formulas are then used to calculate the theory values for the second-order autocorrelation functions according to equations (4) and (5). In figure 7, the theory model for all the different probabilities is shown together with the experimental data.

For a spectrally pure source (i.e. $\lambda_1 = 1$), the derived formulas (A1)–(A5) simplify. In the case of non-unit spectral purity $P = \sum \lambda_k^2 < 1$, but still $P > \frac{1}{2}$, we estimate P by fixing two Schmidt coefficients $\lambda_{1,2} = \frac{1}{2} \pm \sqrt{\frac{P}{2} - \frac{1}{4}}$ and fitting $g^{(2)}_{\mathrm{unc.}}(0) \approx p_{ab}/p_a p_b$ to the experimental value. In our case, we find that the purity of the source decreases as a function of μ, therefore a second-order polynomial is fitted to the purity values obtained from $g^{(2)}_{\mathrm{unc.}}(0)$ to get the function $P_{\mathrm{meas.}}(\mu)$ which is then used throughout in the theoretical model. We attribute the decrease in purity for increasing pump power to the nonlinearity of the spatial mode cleaning fiber in our setup before the nonlinear crystal. This behavior is confirmed by the measurement of the pump spectrum as a function of pump power and a simulation of the corresponding joint spectral amplitude of the down-converted photon pairs [30, 37, 38].

Appendix B. PNR characterization

Here, we report the results of the PNR characterization of the four-pixel P-SNSPD and the full **P** matrix that we obtain following the method described in [24]:

$$\mathbf{P} = \begin{bmatrix} 1 & 0.161 & 0.026 & 0.004 & 0 & 0 & 0 & 0 & 0 & 0 \\ 0 & 0.839 & 0.557 & 0.312 & 0.170 & 0.093 & 0.051 & 0.028 & 0.015 & 0.008 \\ 0 & 0 & 0.417 & 0.600 & 0.640 & 0.619 & 0.576 & 0.526 & 0.478 & 0.433 \\ 0 & 0 & 0 & 0.084 & 0.183 & 0.269 & 0.338 & 0.392 & 0.432 & 0.463 \\ 0 & 0 & 0 & 0 & 0.007 & 0.019 & 0.035 & 0.054 & 0.075 & 0.096 \end{bmatrix}, \tag{B1}$$

where each column indicates the number of photon sent to the detector and each row the number of detected ones.

The single-pixel efficiencies are 3.48%, 33.53%, 41.25% and 5.64%. Since the pixels are distributed one next to the other, the outer ones are naturally less exposed to light (due to the Gaussian beam profile of light in single-mode fibers), thus displaying lower efficiency. These values are used in the theoretical model to calculate η_{h} and the normalized splitting ratios T_i.

ORCID iDs

Lorenzo Stasi https://orcid.org/0000-0002-4623-5599
Patrik Caspar https://orcid.org/0000-0003-1535-9801
Tiff Brydges https://orcid.org/0000-0001-5239-9752
Hugo Zbinden https://orcid.org/0000-0002-9237-1700
Félix Bussières https://orcid.org/0000-0003-0234-175X
Rob Thew https://orcid.org/0000-0003-0188-6053

References

[1] Gisin N and Thew R 2007 Quantum communication *Nat. Photon.* **1** 165–71
[2] Sangouard N, Simon C, De Riedmatten H and Gisin N 2011 Quantum repeaters based on atomic ensembles and linear optics *Rev. Mod. Phys.* **83** 33
[3] Knill E, Laflamme R and Milburn G J 2001 A scheme for efficient quantum computation with linear optics *Nature* **409** 46–52
[4] Kok P, Munro W J, Nemoto K, Ralph T C, Dowling J P and Milburn G J 2007 Linear optical quantum computing with photonic qubits *Rev. Mod. Phys.* **79** 135
[5] Slussarenko S and Pryde G J 2019 Photonic quantum information processing: a concise review *Appl. Phys. Rev.* **6** 041303
[6] Spring J B *et al* 2013 Boson sampling on a photonic chip *Science* **339** 798–801
[7] Bentivegna M *et al* 2015 Experimental scattershot Boson sampling *Sci. Adv.* **1** e1400255
[8] Zhong H-S *et al* 2018 12-photon entanglement and scalable scattershot Boson sampling with optimal entangled-photon pairs from parametric down-conversion *Phys. Rev. Lett.* **121** 250505
[9] Castelletto S and Scholten R 2008 Heralded single photon sources: a route towards quantum communication technology and photon standards *Eur. Phys. J. Appl. Phys.* **41** 181–94
[10] Eisaman M D, Fan J, Migdall A and Polyakov S V 2011 Invited review article: single-photon sources and detectors *Rev. Sci. Instrum.* **82** 071101
[11] Mosley P J, Lundeen J S, Smith B J, Wasylczyk P, U'Ren A B, Silberhorn C and Walmsley I A 2008 Heralded generation of ultrafast single photons in pure quantum states *Phys. Rev. Lett.* **100** 133601
[12] Bruno N, Martin A, Guerreiro T, Sanguinetti B and Thew R T 2014 Pulsed source of spectrally uncorrelated and indistinguishable photons at telecom wavelengths *Opt. Express* **22** 17246
[13] Graffitti F, Barrow P, Proietti M, Kundys D and Fedrizzi A 2018 Independent high-purity photons created in domain-engineered crystals *Optica* **5** 514–7
[14] Meyer-Scott E, Silberhorn C and Migdall A 2020 Single-photon sources: approaching the ideal through multiplexing *Rev. Sci. Instrum.* **91** 041101
[15] Christ A and Silberhorn C 2012 Limits on the deterministic creation of pure single-photon states using parametric down-conversion *Phys. Rev.* A **85** 023829
[16] Lita A E, Miller A J and Nam S W 2008 Counting near-infrared single-photons with 95% efficiency *Opt. Express* **16** 3032–40
[17] Morais L A, Weinhold T, de Almeida M P, Lita A, Gerrits T, Nam S W, White A G and Gillett G 2020 Precisely determining photon-number in real-time (arXiv:2012.10158)
[18] Cahall C, Nicolich K L, Islam N T, Lafyatis G P, Miller A J, Gauthier D J and Kim J 2017 Multi-photon detection using a conventional superconducting nanowire single-photon detector *Optica* **4** 1534–5
[19] Zhu D, Colangelo M, Chen C, Korzh B A, Wong F N, Shaw M D and Berggren K K 2020 Resolving photon numbers using a superconducting nanowire with impedance-matching taper *Nano Lett.* **20** 3858–63
[20] Sempere-Llagostera S, Thekkadath G S, Patel R B, Kolthammer W S and Walmsley I A 2022 Reducing g(2)(0) of a parametric down-conversion source via photon-number resolution with superconducting nanowire detectors *Opt. Express* **30** 3138
[21] Davis S I *et al* 2022 Improved heralded single-photon source with a photon-number-resolving superconducting nanowire detector *Phys. Rev. Appl.* **18** 064007
[22] Marsili F *et al* 2009 Superconducting parallel nanowire detector with photon number resolving functionality *J. Mod. Opt.* **56** 334–44

[23] Perrenoud M, Caloz M, Amri E, Autebert C, Schönenberger C, Zbinden H and Bussières F 2021 Operation of parallel SNSPDs at high detection rates *Supercond. Sci. Technol.* **34** 024002
[24] Stasi L, Gras G, Berrazouane R, Perrenoud M, Zbinden H and Bussières F 2023 Fast high-efficiency photon-number-resolving parallel superconducting nanowire single-photon detector *Phys. Rev. Appl.* **19** 064041
[25] Schmidt M, Von Helversen M, López M, Gericke F, Schlottmann E, Heindel T, Kück S, Reitzenstein S and Beyer J 2018 Photon-number-resolving transition-edge sensors for the metrology of quantum light sources *J. Low Temp. Phys.* **193** 1243–50
[26] Von Helversen M, Böhm J, Schmidt M, Gschrey M, Schulze J-H, Strittmatter A, Rodt S, Beyer J, Heindel T and Reitzenstein S 2019 Quantum metrology of solid-state single-photon sources using photon-number-resolving detectors *New J. Phys.* **21** 035007
[27] Tomm N, Mahmoodian S, Antoniadis N O, Schott R, Valentin S R, Wieck A D, Ludwig A, Javadi A and Warburton R J 2023 Photon bound state dynamics from a single artificial atom *Nat. Phys.* **19** 1–6
[28] Walls D and Milburn G J 2008 *Quantum Optics* (Springer)
[29] Takeoka M, Jin R-B and Sasaki M 2015 Full analysis of multi-photon pair effects in spontaneous parametric down conversion based photonic quantum information processing *New J. Phys.* **17** 043030
[30] Zielnicki K, Garay-Palmett K, Cruz-Delgado D, Cruz-Ramirez H, O'Boyle M F, Fang B, Lorenz V O, U'Ren A B and Kwiat P G 2018 Joint spectral characterization of photon-pair sources *J. Mod. Opt.* **65** 1141–60
[31] Graffitti F, Kelly-Massicotte J, Fedrizzi A and Brańczyk A M 2018 Design considerations for high-purity heralded single-photon sources *Phys. Rev.* A **98** 053811
[32] Klyshko D N 1980 Use of two-photon light for absolute calibration of photoelectric detectors *Sov. J. Quantum Electron.* **7** 1112–6
[33] Zhang W, Huang J, Zhang C, You L, Lv C, Zhang L, Li H, Wang Z and Xie X 2019 A 16-pixel interleaved superconducting nanowire single-photon detector array with a maximum count rate exceeding 1.5 GHz *IEEE Trans. Appl. Supercond.* **29** 1–4
[34] Grünenfelder F *et al* 2023 Fast single-photon detectors and real-time key distillation enable high secret-key-rate quantum key distribution systems *Nat. Photon.* **17** 1–5
[35] Caspar P, Oudot E, Sekatski P, Maring N, Martin A, Sangouard N, Zbinden H and Thew R 2022 Local and scalable detection of genuine multipartite single-photon path entanglement *Quantum* **6** 671
[36] Sangouard N, Simon C, Minář J, Zbinden H, de Riedmatten H and Gisin N 2007 Long-distance entanglement distribution with single-photon sources *Phys. Rev.* A **76** 050301
[37] Guerreiro T, Martin A, Sanguinetti B, Bruno N, Zbinden H and Thew R T 2013 High efficiency coupling of photon pairs in practice *Opt. Express* **21** 27641
[38] Ljunggren D and Tengner M 2005 Optimal focusing for maximal collection of entangled narrow-band photon pairs into single-mode fibers *Phys. Rev.* A **72** 062301